First Paschen α Imaging from the Ground: the First Light of Atacama Near-Infrared Camera on the miniTAO 1m Telescope

Kentaro Motohara[a], Masahiro Konishi[a], Koji Toshikawa[a], Natsuko Mitani[a], Shigeyuki Sako[a], Yuka K. Uchimoto[a], Tomoyasu Yamamuro[b], Takeo Minezaki[a], Toshihiko Tanabe[a], Takashi Miyata[a], Shintaro Koshida[a], Daisuke Kato[c,g], Ryou Ohsawa[c], Tomohiko Nakamura[a], Kentaro Asano[a], Yuzuru Yoshii[a], Mamoru Doi[a], Kotaro Kohno[a], Masuo Tanaka[a], Kimiaki Kawara[a], Toshihiro Handa[a], Tsutomu Aoki[d], Takao Soyano[d], Ken'ichi Tarusawa[d], Yoshifusa Ita[e,f]

[a]Institute of Astronomy, University of Tokyo, Osawa 2-21-1, Mitaka, Tokyo 181-0015, Japan;
[b]OptCract, Higashi Hashimoto 3-16-8-101, Midori-ku, Sagamihara, Kanagawa 229-1104, Japan;
[c]Department of Astronomy, University of Tokyo, Hongo 7-3-1, Bunkyo-ku, Tokyo 113-0033, Japan;
[d]Kiso Observatory, University of Tokyo, Mitake 10762-30, Kiso, Nagano 397-0101, Japan;
[e]National Astronomical Observatory, Osawa 2-21-1, Mitaka, Tokyo 181-8588, Japan;
[f]Astronomical Institute, Tohoku University, Aramaki 6-3, Aoba-ku, Sendai, Miyagi 980-8578, Japan;
[g]Institute of Space and Astronautical Science,Yoshinodai 3-1-1, Chuo-ku, Sagamihara, Kanagawa 252-5210, Japan;

ABSTRACT

We have developed a near infrared camera called ANIR (Atacama Near InfraRed camera) for the University of Tokyo Atacama 1.0m telescope installed at the summit of Co. Chajnantor (5640m altitude) in northern Chile. The camera is based on a PACE HAWAII-2 array with an Offner relay optics for re-imaging, and field of view is $5\farcm3 \times 5\farcm3$ with pixel scale of $0\farcs31$/pix. It is also capable of optical/infrared simultaneous imaging by inserting a dichroic mirror before the focal plane. The high altitude and extremely low water vapor (PWV=0.5mm) of the site enables us to perform observation of hydrogen Paschen-α (Paα) emission line at 1.8751 μm. The first light observation was carried out in July 2009, and we have successfully obtained Paα images of the Galactic center using the $N1875$ narrow-band filter. This is the first success of Paα imaging of a Galactic object from a ground based telescope. System efficiencies for the broad-band filters are measured to be 15% at the J-band and 30% at Ks, while that of the $N1875$ narrow-band filter, corresponding to Paα wavelength, varies from 8 to 15%, which may be caused by fluctuation of the atmospheric transmittance. ATRAN simulation suggests that this corresponds to PWV of 0.3 – 1.5mm, consistent with previous results of the site testing. Measured seeing size is median $\sim0\farcs8$, corresponding to the real seeing value of $0\farcs6$ – $0\farcs8$. These results demonstrates the excellent capability of the site for infrared observations.

Keywords: near infrared, imager, Paschen alpha, PWV, Atacama, Co. Chajnantor

1. INTRODUCTION

Institute of Astronomy, University of Tokyo is planning to construct a 6.5m infrared-optimized telescope at the summit of Co. Chajnantor (5640m altitude) in northern Chile, which is called the University of Tokyo Atacama Observatory Project.[1,2] The site has ideal weather condition for the infrared astronomy; high clear fraction (>80% usable[3]), low perceptible water vapor (PWV : 0.5mm at 25%-tile[4]), and good seeing ($<0\farcs7$ in the V-band[5]).

Especially, the low PWV invokes high atmospheric transmittance and almost continuous transmission in the near-infrared wavelength is achieved. As a result, observation of hydrogen Paschen-α (Paα) emission line at 1.8751μm becomes possible. Paα is the strongest hydrogen line in the near-infrared wavelength. Having strong penetrating power, it is an ideal probe for star formation activities hidden behind thick interstellar dust clouds such as HII regions in the Galactic disk and dusty starburst galaxies. However, because of poor atmospheric

Further author information: K.M.: E-mail: kmotohara@ioa.s.u-tokyo.ac.jp, Telephone: 81 422 34 5039

Ground-based and Airborne Instrumentation for Astronomy III, edited by Ian S. McLean, Suzanne K. Ramsay, Hideki Takami, Proc. of SPIE Vol. 7735, 77353K · © 2010 SPIE · CCC code: 0277-786X/10/$18 · doi: 10.1117/12.856102

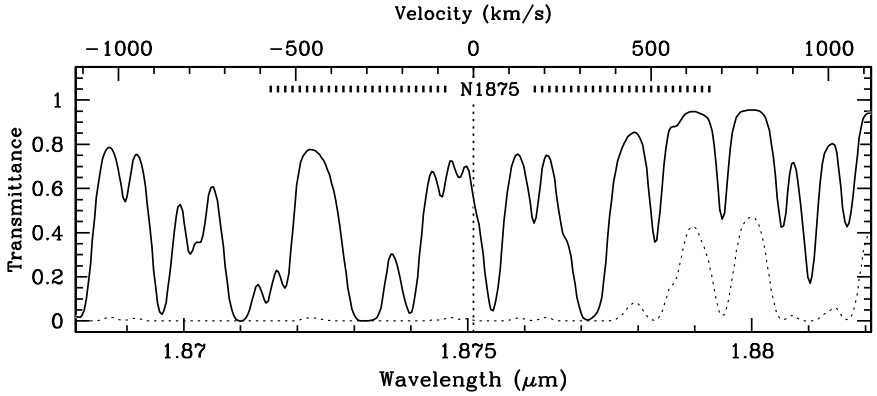

Figure 1. Simulated atmospheric transmittance by the ATRAN atmospheric model.[8] Solid line shows that at Co. Chajnantor(5640m) assuming PWV=0.5mm, and dotted line at 2600m altitude with PWV=2.6mm. Vertical dotted lines show the wavelength of hydrogen Paα emission line (1.8751μm). Horizontal thick dotted line indicates the wavelength range of the narrow-band filter $N1875$.

transmittance, no Paα imaging of a Galactic object from a ground-based telescope is reported so far. Figure 1 shows the transmittance at the wavelength of Paα. While almost no Paα photon reaches the ground at 2600m altitude (this is the height of major observatories in the southern hemisphere), transmittance over 50% is expected at Co. Chajnantor.

As a pathfinder of the TAO 6.5m telescope, we have installed the University of Tokyo Atacama 1.0m telescope (miniTAO 1.0m)[6,7] at the summit of Co. Chajnantor in 2009, started scientific observation using the Atacama Near InfraRed camera (ANIR), and successfully obtained Paα images of Galactic objects from the ground. In this presentation, we report the performance of ANIR at the 5640m altitude, mainly focusing on the Paα imaging capability.

2. ATACAMA NEAR-INFRARED CAMERA

2.1 Near-Infrared Imager Unit

Figure 2 shows the overall layout of ANIR. The main body of ANIR is a near-infrared (NIR) imager unit, contained in a cubic cryostat with ∼260mm on a side. This NIR unit is based on an engineering grade PACE HAWAII-2 array detector, with an Offner relay optics for re-imaging. Two filter wheels, containing 4 filters each, are located just after the telescope focal plane. They are driven by cryogenic motors which are remodeled from non-cryogenic products by replacing their ball bearings with those with MoS_2 sputtered bearing balls. The wheels contain 4 broad-band Y, J, H, Ks filters of Mauna Kea observatories infrared filter set[9,10] and 4 narrow-band filters. All the cryogenic components are cooled by a GM closed cycle cooler, which is electrostatically insulated from the cryostat by inserting a sapphire plate at the cold head and a Teflon plate at the base plate of the housing. The detector is driven by data acquisition system TAC[11] based on a Linux PC and a commercial digital I/O board. Out of 2048×2048 pixels of the array detector, only a single quadrant of 1024×1024 pixels is

Table 1. Specifications of ANIR NIR Unit.

Detector	PACE HAWAII-2
Pixel Format	1024 × 1024
Pixel Scale	$0\overset{''}{.}31$/pix
Field of View	$5\overset{'}{.}3 \times 5\overset{'}{.}3$
Readout Noise	<15 e$^-$ r.m.s. (at 4μs/pix sampling)
Filters	Y, J, H, Ks, $N128$, $N1875$, $N191$, $N207$

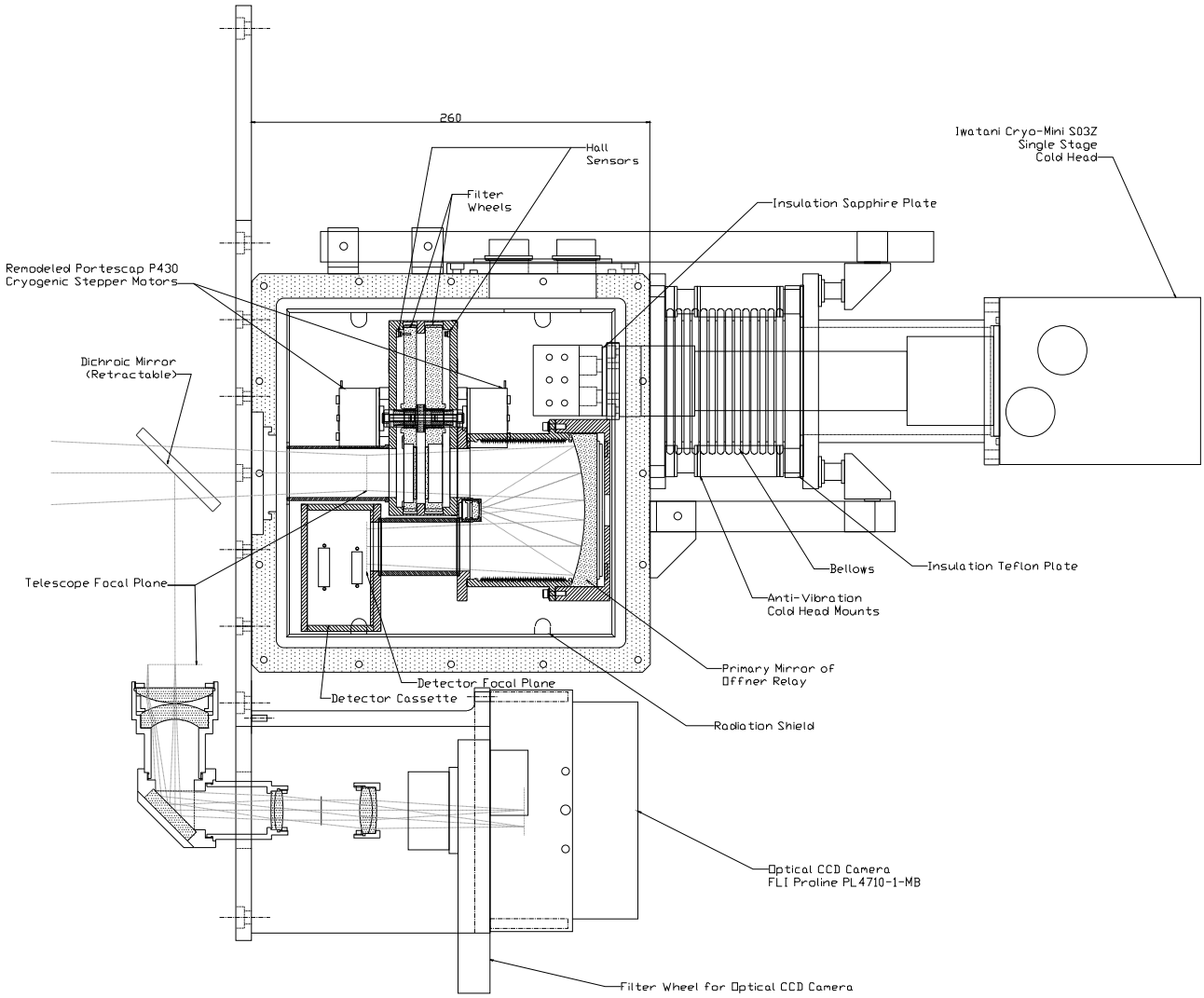

Figure 2. Layout of ANIR.

used with a single readout mode. Default readout speed is 4μs/pix which results in the minimum exposure time of 4.2sec. For detailed information, see Motohara et al. 2008.[12] Specifications are summarized in Table 1.

2.2 Narrow-band Filters

The NIR unit is equipped with four narrow-band filters designed and fabricated by Optical Coatings Japan, which are $N128$ (λ=1.281μm, $\Delta\lambda$=0.0214μm) for Paβ λ1.2818μm, $N1875$ (λ=1.8754μm, $\Delta\lambda$=0.0079μm) for Paα λ1.8751μm, , $N191$ (λ=1.910μm, $\Delta\lambda$=0.033μm) for off-band imaging of Paα, and $N207$ (λ=2.074μm, $\Delta\lambda$=0.041μm). Figure 3 shows the filter profiles of $N1875$ and $N191$, together with the simulated atmospheric transmittance at the summit of Co. Chajnantor.

2.3 Optical Imaging Unit

By inserting a dichroic mirror before the cryostat window of the NIR unit, ANIR is capable of optical and NIR simultaneous imaging. The dichroic mirror, fabricated by Asahi Spectra Co., has a dimension of 50mm $\times$ 71mm $\times$ 10mm with a wedge angle of 0.53° to minimize astigmatism in the NIR image. Its transmittance is > 0.9 at 0.95–2.4μm, while reflectance of > 0.9 is achieved at 0.4–0.86μm with the incident angle of 45°. It is installed

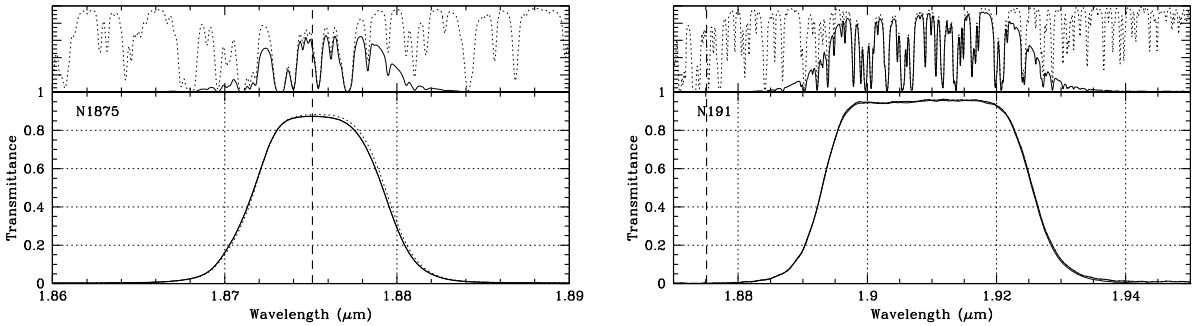

Figure 3. The lower plots of both panels show filter profiles of the $N1875$ (left) and the $N191$ (right) narrow-band filters at 77K (solid lines) and 300K (dotted lines). The upper plots show simulated atmospheric transmittance at 5600m with PWV=0.5mm (dotted line) and effective filter profile (solid line).

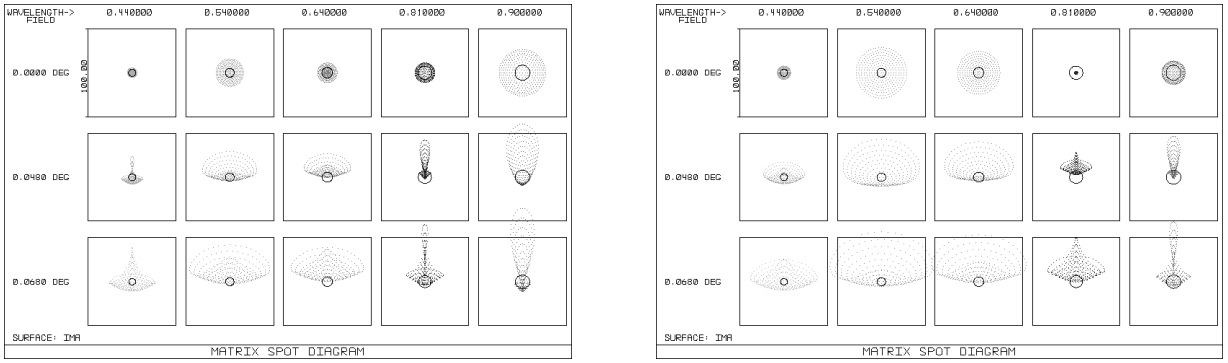

Figure 4. (Left) Spot diagrams of the optical imaging unit. Wavelength varies from 0.44μm, 0.54μm, 0.64μm, 0.81μm, and 0.90μm from left to right, with the spots at the field center shown in the top line, at $2\farcm9$ from the center in the middle, and at the edge of the field of view in the bottom. Each box is 100μm on a side, corresponding to $2\farcs5$. (Right) Same as the left panel, except the focal position offset by 0.2mm.

on a movable stage, and can be retracted to achieve better image quality, higher efficiency, and lower thermal background in the NIR when no simultaneous imaging is necessary.

The reflected light by the dichroic mirror enters a re-imaging refractive optics, and is focused on a CCD camera unit with final F of 7.9. Figure 4 shows spot diagrams at the final focal plane. Due to chromatic aberration of the optics, the focal position is offset by $\sim$0.2mm in the I-band, which can be compensated by shifting the refocus lens unit.

We incorporate a commercial CCD camera unit Proline PL4710-1-BF fabricated by Finger Lakes Instrumentation, which adopts an E2V backside illuminated CCD. A filter wheel containing 4 broad-band B, V, R, and I filters of Johnson system is located in front of the CCD camera unit. In addition to these filters, a grism with 75 lines/mm will be installed by the end of 2010. It enables us to carry out slitless spectroscopy, which will achieve wavelength resolution of $R \sim 50$. Both the CCD camera unit and the filter wheel are controlled from a host Linux PC via USB interface. Table 2 summarizes the specification of the optical imaging unit.

3. PERFORMANCE ON THE TELESCOPE

ANIR saw the first light on July 9, 2009 at the miniTAO 1.0m telescope. Figure 5 shows ANIR installed on the Cassegrain focus of the telescope.

3.1 Paschen α Emission-Line Imaging

On July 10, 2009, we have carried out Paα imaging of the Galactic center (Sgr A*) using the $N1875$ filter, and successfully obtained the image shown in Figure 6. This is the first Paα imaging observation of a Galactic object

Table 2. Specifications of ANIR Optical Unit.

Detector	E2V backside illuminated CCD
Pixel Format	1024×1024
Pixel Size	13.5μm
Pixel Scale	$0\overset{''}{.}34$/pix
Field of View	$5\overset{'}{.}8 \times 5\overset{'}{.}8$
Readout Noise	14 e^- r.m.s.
Filters	B, V, R, I (Johnson System)

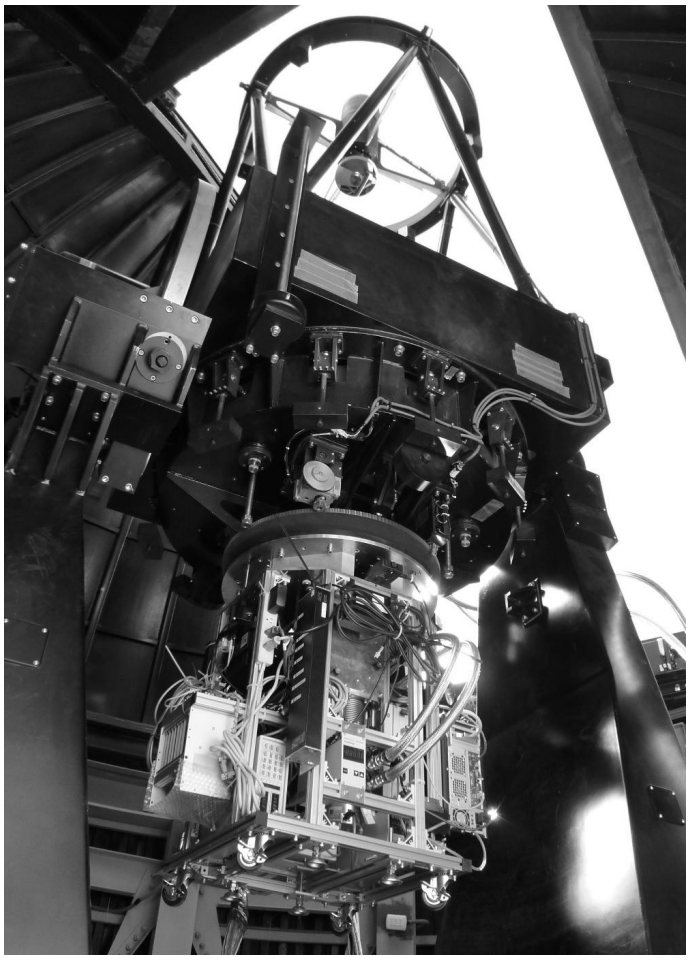

Figure 5. ANIR installed at the Cassegrain focus of the University of Tokyo Atacama 1.0m telescope.

Figure 6. Continuum subtracted Paα emission line image of Sgr A*.

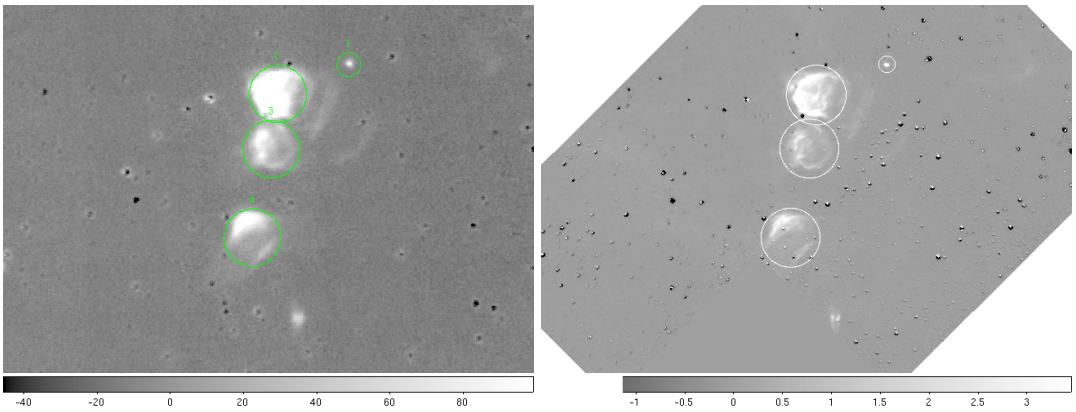

Figure 7. Close-up of the emission-line clouds near Sgr A*, taken by ANIR/miniTAO 1.0m with 1080sec exposure (left), and by HST/NICMOS with 191sec exposure (right). Circles show apertures used to measure the Paα transmittance.

from the ground, demonstrating the high transmittance for Paα photons at the site. Direct comparison with results of Paα imaging survey by HST/NICMOS[13] shows that most of the emission-line components around Sgr A* are detected by ANIR. The sensitivity is comparable with that of HST/NICMOS, especially for extended objects, which can be seen in Figure 7. However, there are some components detected by HST/NICMOS, that are faint or not detected by ANIR. This may be caused by the strong wavelength dependence of the atmospheric transmission profile near 1.8751μm, where even a velocity shift of several$\times$10km/s may result in reduction of the transmittance down to few % as seen in Figure1.

The atmospheric transmittance for Paα photons are measured using the emission-line clouds in Figure 7 by comparing with the HST/NICMOS image. The obtained values vary from 15 to 54%, which are consistent with the ATRAN simulation with PWV=0.5mm assuming reasonable velocity offsets of several$\times$10km/s.

3.2 System Efficiencies

Figure 8 shows system efficiencies of ANIR on the miniTAO 1.0m telescope. The NIR efficiencies are measured from 2MASS stars in the observed fields of NIR data, by comparing the number of detected electrons with that of photons from a star. The optical efficiencies are obtained from standard-star frames in the same manner. Each point is average of all measured frames, and the error bar shows its 1 σ dispersion. The efficiencies become 7–10% lower when the dichroic mirror is inserted.

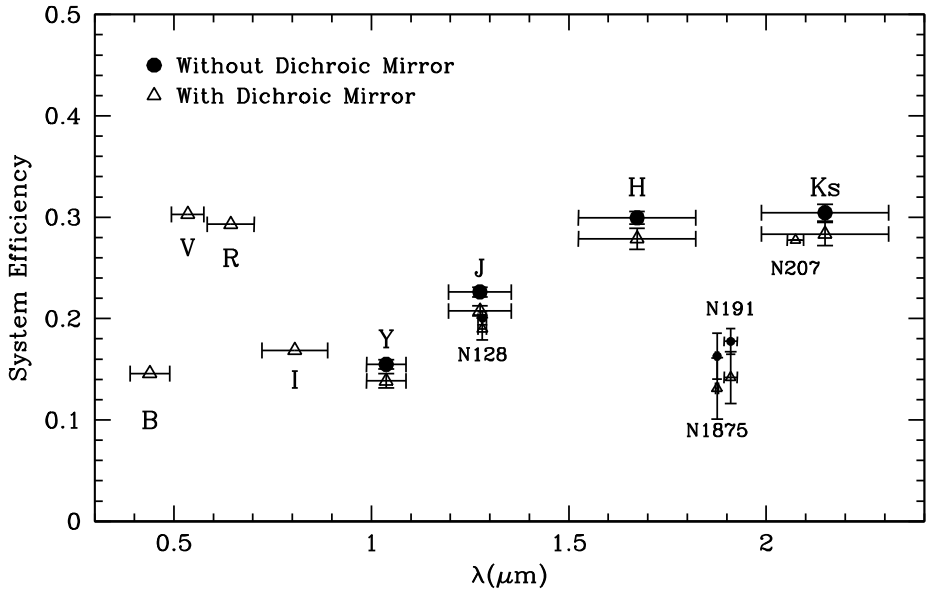

Figure 8. System efficiencies of ANIR. Filled circles shows those without the dichroic mirror, and open triangle with it.

The efficiencies of the $N1875$ and $N191$ narrow-band filters are lower than those of the broad-bands, which is clearly the result of the lower atmospheric transmittance as seen in Figure 3. In addition, even taken on photometric nights, dispersion of the efficiencies is quite large, which may be caused by fluctuation of PWV in the atmosphere.

3.3 PWV and System Efficiencies of Narrow-Band Filters

To check the effect of PWV fluctuation on the atmospheric transmittance, we plot PWV vs. system efficiencies of the $N1875$ and $N191$ filters in Figure 9. Because there are no PWV monitor at the summit, we used PWV data measured by a radiometer of Atacama Pathfinder Experiment (APEX) in the ALMA site at 5100m altitude, near Co. Chajnantor. Clear correlations are seen for both the $N1875$ and $N191$ filters. Also, we have plotted relations obtained from the ATRAN simulation, assuming the efficiency of the telescope and the instrument to be 0.3, the value obtained for the broad-band H and Ks filters. Then, the simulated relations show lower PWV than the measured values for the both filters. If we adopt the simulated PWV-efficiency relation, the measured efficiencies corresponds to PWV of 0.4 – 1mm for the $N1875$ filter and 0.3 – 1.5mm for the $N191$ filter, which is consistent with the value obtained from the satellite data.[4] In addition to this, some data points show large deviations having high ($>$ 2mm) PWV with rather high efficiency (10–15%).

These results suggest that PWV at the summit is lower than that measured at APEX where the altitude is lower by 500m. This is because the atmospheric inversion layer may be lowered below the summit during the night time, and most of the water vapor may be accumulated near the surface of flat terrain of the ALMA site, where APEX is located. Therefore, lower PWV can be expected at the summit of Co. Chajnantor than at the plateau of the ALMA site. Direct PWV measurement at the summit is obviously necessary for confirmation.

3.4 Seeing Statistics

Figure 10 shows seeing statistics, where median seeing is $\sim 0\overset{''}{.}8$ for all the broad-band filters. Considering the diffraction-limited image size and Hartmann constant ($0\overset{''}{.}19$) of the telescope optics,[7] they correspond to the real seeing values of $0\overset{''}{.}76$ – $0\overset{''}{.}64$ at $Y - Ks$ band, respectively. The best seeing in the optical channel is also good as $0\overset{''}{.}7$. These results are consistent with the value obtained by seeing-monitor observations, which is median $\sim 0\overset{''}{.}69$ in the V-band.[5]

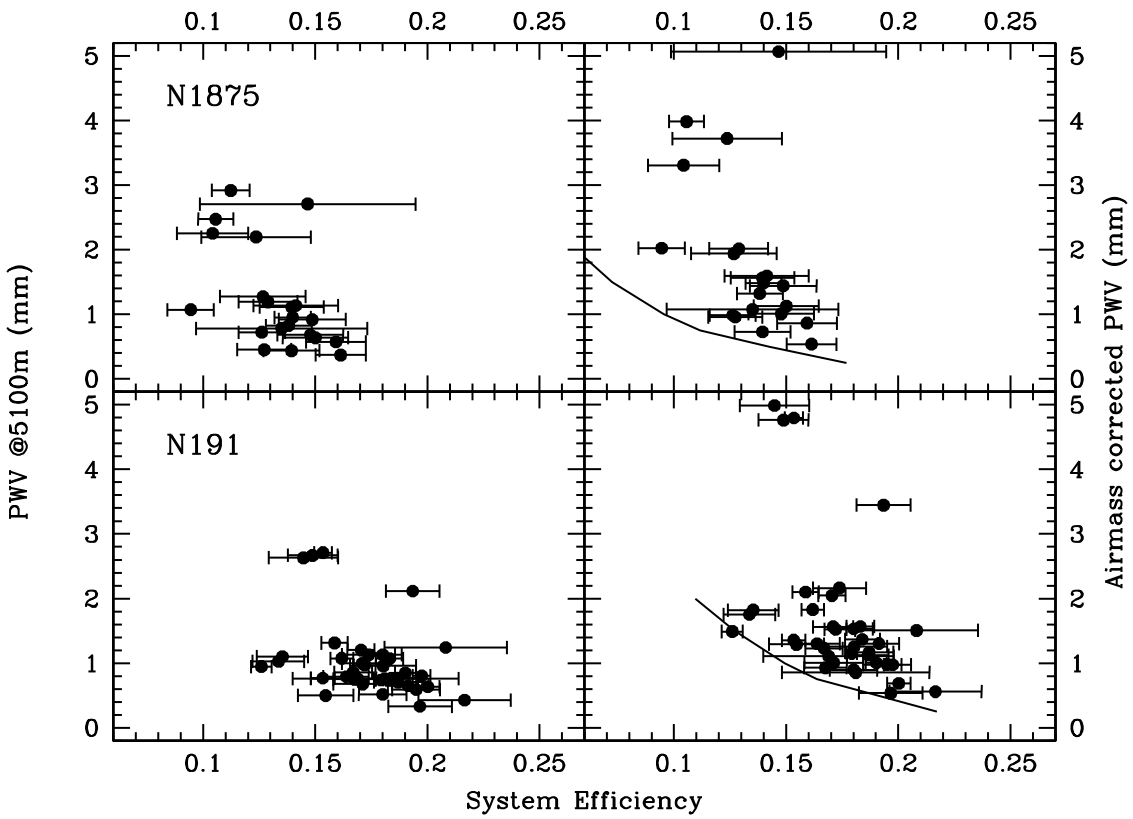

Figure 9. Correlations between system efficiencies and PWV measured at a 5100m site . Upper panels show those for the $N1875$ filter and lower for the $N191$. Left panels compare the efficiency with the measured PWV, while the right with the PWV rescaled for airmass of the target. Solid lines are relation from the ATRAN simulation, assuming the efficiency of the instrument and the telescope to be 0.3.

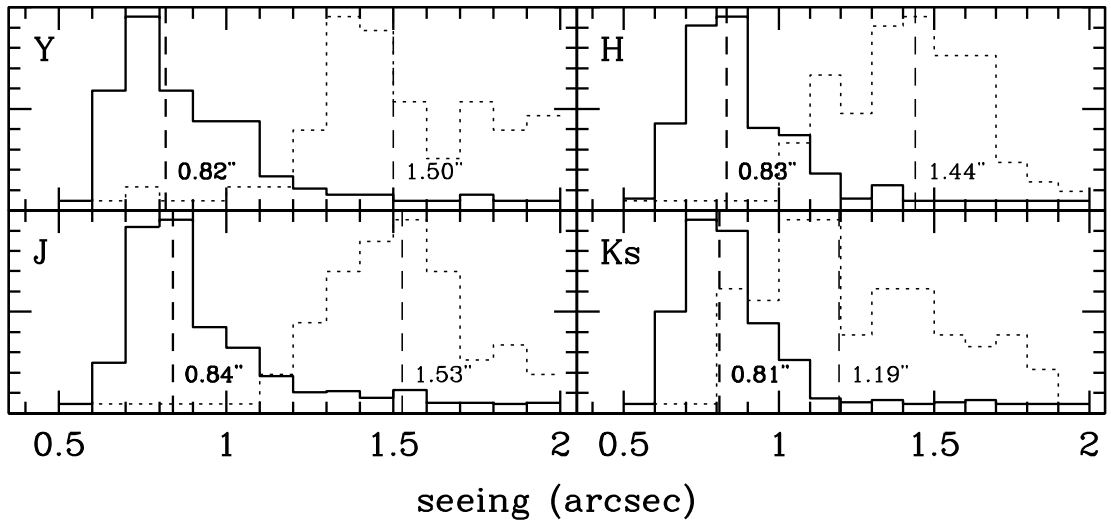

Figure 10. Seeing statistics of ANIR/miniTAO 1.0m. Solid lines show those without the dichroic mirror and dotted lines with it. Vertical lines show median values.

Table 3. 5σ limiting magnitudes of ANIR. All magnitudes are in AB system, with 600sec exposure and $1\overset{''}{.}8$ diameter aperture.

Band	Limiting Magnitude
Y	20.5
J	20.7
H	20.3
Ks	20.5
$N128$	19.0
$N1875$	16.6
$N191$	18.7

The seeing becomes worse than $1\overset{''}{}$ when the dichroic mirror is inserted. Because this is not expected from a ray-trace simulation[12] and there are some cases when the seeing is as good as $0\overset{''}{.}8$ even with the dichroic mirror, it is not likely that this is caused by optical aberration. Further observations for more statistics are necessary.

3.5 Limiting Magnitudes

Limiting magnitude is measured from a final image obtained during the observational run, by performing random aperture photometry of blank sky region and calculating its standard deviation. Results are shown in Table 3. Note that they are typical values and some of them vary by 0.5mag maximum due to fluctuation of background emission such as OH airglows and thermal emission from the telescope or the atmosphere. In addition, the variation of the atmospheric transmittance in the $N1875$ and $N191$ narrow-band filters, caused by the PWV fluctuation, is another cause of uncertainty.

ACKNOWLEDGMENTS

This research is supported by Ministry of Education, Culture, Sports, Science and Technology of Japan, Grant-in-Aid for Scientific Research (17104002, 20040003, 20041003, 21018003) from the JSPS of Japan. Part of this work has been supported by National Astronomical Observatory of Japan (NAOJ) Research Grant for Universities. Part of the ANIR development was supported by the Advanced Technology Center, NAOJ. The HAWAII-2 array detector has been generously leased by Subaru Telescope, NAOJ. The NICMOS data presented is based on observations made with the NASA/ESA Hubble Space Telescope, obtained from the data archive at STScI. STScI is operated by the Association of Universities for Research in Astronomy, Inc. under NASA contract NAS 5-26555. We thank Atacama Pathfinder Experiment for providing their radiometer data on the web.

REFERENCES

[1] Yoshii, Y., Doi, M., Handa, T., Kawara, K., Kohno, K., Minezaki, T., Mitsuda, K., Miyata, T., Motohara, K., and Tanaka, M., "Tokyo Atacama Observatory Project," *Proceedings of the IAU 8th Asian-Pacific Regional Meeting* **II**, 35–36 (2002).

[2] Yoshii, Y., Aoki, T., Doi, M., Handa, T., Kawara, K., Kato, D., Kohno, K., Konishi, M., Koshida, S., Minezaki, T., Mitani, N., Miyata, T., Motohara, K., Sako, S., Soyano, T., Tanabe, T., Tanaka, M., Tarusawa, K., Bronfman, L., Luiz, M. T., and Hamuy, M., "The University of Tokyo Atacama Observatory 6.5m Telescope Project," *Proc. SPIE* (2010).

[3] Miyata, T., Motohara, K., Sako, S., Tanaka, M., Minezaki, T., Mitani, N., Aoki, T., Soyano, T., Tanabe, T., Kawara, K., Kohno, K., Tarusawa, K., Handa, T., Doi, M., Yoshii, Y., Ezawa, H., Bronfman, L., and Ruiz, M. T., "Site Evaluations of the Summit of Co. Chajnantor for Infrared Observations," in [*Ground-based and Airborne Telescopes II*], Stepp, L. M. and Gilmozzi, R., eds., *Proc. SPIE* **7012**, 701243 (2008).

[4] Erasmus, D. A. and van Staden, C. A., "A Satellite Survey of Cloud Cover and Water Vapor in Northern Chile," A study conducted for Cerro Tololo Inter-American Observatory and University of Tokyo (2001).

[5] Motohara, K., Aoki, T., Sako, S., Soyano, T., Doi, M., Tanaka, M., Tanabe, T., Handa, T., Mitani, N., Minezaki, T., Miyata, T., Kawara, K., Kohno, K., Tarusawa, K., Yoshii, Y., Bronfman, L., Ruiz, M. T., Uraguchi, F., and Takato, N., "Seeing environment at a 5640m altitude of Co. Chajnantor in northern Chile," in [*Ground-based and Airborne Telescopes II*], Stepp, L. M. and Gilmozzi, R., eds., *Proc. SPIE* **7012**, 701244 (2008).

[6] Sako, S., Aoki, T., Doi, M., Handa, T., Kawara, K., Kohno, K., Minezaki, T., Mitani, N., Miyata, T., Motohara, K., Soyano, T., Tanabe, T., Tanaka, M., Tarusawa, K., Yoshii, Y., Bronfman, L., and Ruiz, M. T., "The University of Tokyo Atacama 1.0-m Telescope," in [*Ground-based and Airborne Telescopes II*], Stepp, L. M. and Gilmozzi, R., eds., *Proc. SPIE* **7012**, 70122T (2008).

[7] Minezaki, T., Kato, D., Sako, S., Konishi, M., Koshida, S., Mitani, N., Aoki, T., Doi, M., Handa, T., Ita, Y., Kawara, K., Kohno, K., Miyata, T., Motohara, K., Soyano, T., Tanabe, T., Tanaka, M., Tarusawa, K., Yoshii, Y., and Bronfman, L., "The University of Tokyo Atacama 1.0-m Telescope," *Proc. SPIE* (2010).

[8] Lord, S. D., "A new software tool for computing Earth's atmospheric transmission of near- and far-infrared radiation," Technical Memorandum 103957, NASA (1992).

[9] Tokunaga, A. T., Simons, D. A., and Vacca, W. D., "Mauna Kea Observatories Near-Infrared Filter Set. II. Specifications for a New $JHKL'M'$ Filter Set for Infrared Astronomy," *PASP* **792**, 180–186 (2002).

[10] Simons, D. A. and Tokunaga, A. T., "Mauna Kea Observatories Near-Infrared Filter Set. I. Defining Optimal 1–5 Micron Bandpasses," *PASP* **792**, 169–179 (2002).

[11] Sako, S., Miyata, T., Nakamura, T., Motohara, K., Uchimoto, Y. K., Onaka, T., and Kataza, H., "Developing infrared array controller with software real time operating system," in [*High Energy, Optical, and Infrared Detectors for Astronomy III*], Dorn, D. A. and Holland, A. D., eds., *Proc. SPIE* **7021**, 702128 (2008).

[12] Motohara, K., Mitani, N., Sako, S., Uchimoto, Y. K., Toshikawa, K., Yamamuro, T., Handa, T., Tanaka, M., Aoki, T., Doi, M., Kawara, K., Kohno, K., Minezaki, T., Miyata, T., Soyano, T., Tanabe, T., Tarusawa, K., and Yoshii, Y., "ANIR: Atacama Near Infrared Camera for Paschen α Imaging," in [*Ground-based and Airborne Instrumentation for Astronomy II*], McLean, I. S. and Casali, M. M., eds., *Proc. SPIE* **7014**, 70142T (2008).

[13] Wang, Q. D., Dong, H., Cotera, A., Stolovy, S., Morris, M., Lang, C. C., Muno, M. P., Schneider, G., and Calzetti, D., "HST/NICMOS Paschen-α Survey of the Galactic Centre: Overview," *MNRAS* **402**, 895–902 (2010).